Indian Journal of Chemistry
Vol. 65, March 2026, pp. 227-235
DOI: 10.56042/ijc.v65i3.22128

Copper (II) complexes supported by phenyl selanyl ligands: DNA binding and molecular docking studies

P Moohambihai*[a], A Sivasubramanian[b] & R Maheswaran[c]

[a] Department of Chemistry, V V College of Engineering, Tisaiyanvilai 627 657, Tamil Nadu, India

[b] Department of Mechanical Engineering, V V College of Engineering, Tisaiyanvilai 627 657, Tamil Nadu, India

[c] Department of Mechanical Engineering, Mepco Schlenk Engineering College, Virudhunagar 626 005, Tamil Nadu, India

E-mail: ambikachem12@gmail.com

Received 29 July 2025; accepted (revised) 6 March 2026

Copper (II) complexes (**3a-d**) with (16E)-2,6-dimethyl-N-(2-phenylquinoline-4(1*H*)-ylidene)-5-(phenylselanyl) pyrimidine-4-amine ligands have been developed. They have been characterised by elemental analysis and several spectroscopic studies. Absorption spectra, fluroscence investigations, and viscosity tests reveal how the copper complexes interact with the calf thymus (CT-DNA). Furthermore, the ligand's ability to inhibit acetylcholinesterase (AChE) has been studied in order to establish its efficacy in the treatment of neurodegenerative diseases. Compared to normal Rivastigmine and Galantamine, the synthesised ligand **2c** shows selective inhibition (AChE and BuChE) with IC50 values of 0.18 and 3.03 μM. A molecular docking study has been carried out.

Keywords: Copper (II) complexes, Selenium, Acetylcholinesterase, Quinoline, Alzheimer's disease

Schiff bases bind redox active transition metal ions *via* the -CH=N or Ar-O- atoms[1-3]. They are used in a variety of fields, including pharmaceuticals[4-7], catalysts[8-10], polymer synthesis, energy[11] and industrial chemistry[12]. Copper, Cobalt, Nickel, and Zinc complexes are the most attractive transition metals due to their redox behavior, low toxicity, and existence in biological molecules[13]. Chemical structural changes to known therapeutic molecules are an important approach to the drug development process. Heterocyclic moieties, which are found in a wide range of chemicals, play a vital part in a number of biological processes[14]. These compounds' molecular structures are primarily responsible for their biological activity. Quinoline core, a nitrogen-containing scaffold, is a powerful pharmacophoric moiety in current drug molecules[15–17]. When selenium combines with quinoline, it becomes active in the research area. The selenium atom is also known to play an important role in the mode of action of certain proteins, something that its closest relative, sulfur, cannot do[18]. Synthetic organoselenium compounds have also been found to act as chemopreventers, apoptosis inducers, and antioxidants in a number of organs, including the brain, liver, skin, colon, lung, prostate, and liver[19,20]. The selenium atom is a useful building block for creating a range of heterocyclic compounds with five and six members that need further study. Alzheimer's disease is a degenerative illness that causes memory loss, cognitive decline, and other mental health problems. Currently, it affects almost 50 million people worldwide and ranks as the sixth most deadly disease. As the disease progressed, alterations in AChE and BuChE activity were seen in the hippocampus and cerebral cortex[21,22]. Many AChE inhibitors have been studied, and researchers are still working to develop some new pharmacologically profiled drug molecules[23,24]. Because of the neurotransmitter acetylcholine deficiency in the brain, AChE and BuChE levels are vary irregularly in Alzheimer's disease. With a better understanding of the relationship between AChE and BuChE levels, Alzheimer's disease can be easily tracked and managed. The majority of drugs available on the market for potential treatment of AD are cholinesterase inhibitors (Galantamine, Donepezil, Rivastigmine). Inhibitors of cholinesterase that block both AChE and BuChE, as well as highly selective BuChE inhibitors, could be useful in treating Alzheimer's disease and other dementias. Both enzymes are still important targets in therapeutic development for Alzheimer's disease. The difficult task is always to create a redox

active and conjugated planar molecule with improved bioactivity against a certain target. Our research focused on new cholinesterase inhibitors as potential anti-multifunctional Alzheimer's therapies. This paper describes the synthesis and spectroscopic elucidation of copper chelates. Several spectroscopic techniques were used to characterize the prepared complexes. DNA binding acetylcholinesterase activities were studied, as well as molecular docking investigations of phenylselanyl quinoline derivatives and chelates were performed.

Experimental Section

In this experiment, AnalaR-grade substances were used. Tetramethylsilane (TMS) served as an internal standard for recording the ligand NMR spectra. In contrast to TMS, chemical changes (δ) are quantified in parts per million. The Fast Atom Bombardment mass spectra (FAB) of the ligands and their complexes were acquired using a Jeol SX 102/DA-6000 mass spectrometer/data system and argon/ xenon (6 kV, 10 mA) as the FAB gas. The molar conductance of copper complexes in dimethyl-sulphoxide (DMSO) solution was determined using a calibrated digital conductivity meter. The IR spectra of the ligands and their copper complexes were measured in the 4000-200 cm^{-1} range using a Perkin-Elmer 783 spectrophotometer, with adjustments performed using Pascal's constant and KBr disc. The magnetic susceptibility values were determined with the equation eff = 2.83 (m.T)1/2. The diamagnetic and calibrant were $Hg[Co(SCN)_4]$. The ESR spectra of the copper complexes were measured at 300 and 77 K using a Varian E112 X-band spectrometer.

Preparation of ligands 2a-d

In 50 mL of DMF, 2,6-dimethyl-5-(phenylselanyl) pyrimidin-4-amine was combined with 12 mmol of sodium borohydride and agitated continuously at 0-5°C. After diluting with an equal volume of DMF, 10 mmol of phenylquinoline compounds 1(a-d) were added drop by drop to the resultant solution. Reactions were completed within 60-90 minutes. The extractions were performed in dichloromethane under vacuum. The organic layer was rinsed multiple times with brine solution before drying on anhydrous sodium sulphate. The solvent was extracted using a rota evaporator, and the liquid was purified using a silica column with chloroform-methanol (8:2) as the eluant (Scheme 1).

(16*E*)-2,6-Dimethyl-N-(2-phenylquinoline-4(1*H*)-ylidene)-5-(phenylselanyl) pyrimidine-4-amine, 2a: Yield 70%. Anal. Calcd for $C_{27}H_{22}N_4Se$: C, 69.03; H, 4.33; N, 9.29. Found: C, 69.01; H, 4.31; N, 9.27%. FAB mass spectrometry (FAB-MS): *m/z* 483 [M+1]; ^{1}H NMR (400 MHz, $CDCl_3$): δ 2.28 (s, 6H), 6.11 (s, 1H), 6.48-6.53 (m, 5H), 7.24-7.26 (d, 2H), 7.58-7.62 (m, 3H), 8.21-8.62 (m, 4H), 8.68 (s, -NH); ^{13}C NMR (400 MHz, DMSO-d_6): δ 138.1 (C-2), 102.1 (C-3), 164.4 (C-4), 129.8 (C-5), 118.7 (C-6), 131.6 (C-7), 116.1 (C-8), 147.8 (C-9), 117.6 (C-10), 134.2 (C-11), 126.2 (C-12, C-16), 128.5 (C-13, C-15), 127.8 (C-14). 181. 8 (C-18), 167.8 (C-20), 165.8 (C-22), 110.7 (C-23), 129.8 (C-25), 131.4 (C-26, C-30), 128.6 (C-27, C-28, C-29), 25.3 (CH3 – C), 21.2 (CH_3 – C); FTIR (KBr): 3310 (N–H), 1638 cm^{-1} (C=N).

(4*E*)-4-(2,6-Dimethyl-5-(phenylselanyl)zpyrimidin-4-ylimino)-1,4-dihydro-2-phenylquinolin-7-ol, 2b: Yield 69%. Anal. Calcd for $C_{27}H_{22}N_4OSe$: C, 65.19; H, 4.46; N, 11.26. Found: C, 65.16; H, 4.42; N, 11.22%. FAB mass spectrometry (FAB-MS): *m/z* 499 [M+1]. ^{1}H NMR (400 MHz, $CDCl_3$): δ 2.28 (s, 6H), 6.11 (s, 1H), 6.22 (d, 1H), 6.38 (d, 1H) 6.46-6.52 (m, 5H), 6.72(s, 1H), 7.22-7.25 (d, 2H), 7.56-7.60 (m, 3H). 8.64 (s, NH), 9.78 (s, -OH); ^{13}C NMR (400

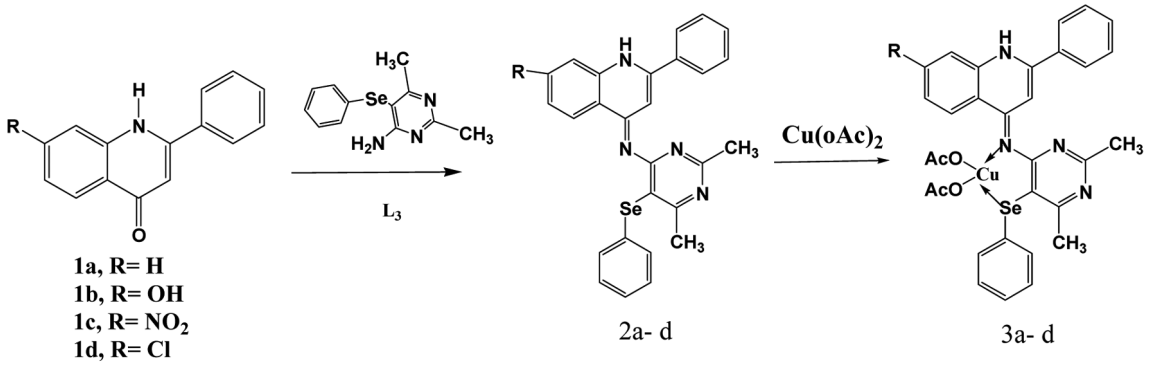

Scheme 1 — Scheme for preparation of ligands **2a-d**

MHz, DMSO-d_6): δ 138.1 (C-2), 102.1 (C-3), 164.4 (C-4), 131.2 (C-5), 105.7 (C-6), 161.4 (C-7), 101.1 (C-8), 149.2 (C-9), 110.2 (C-10), 134.2 (C-11), 126.2 (C-12, C-16), 128.5 (C-13, C-15), 127.8 (C-14). 181. 8 (C-18), 167.8 (C-20), 165.8 (C-22), 110.7 (C-23), 129.8 (C-25), 131.4 (C-26, C-30), 128.6 (C-27, C-28, C-29), 25.3 (CH_3 – C_{20}), 21.2 (CH_3 – C_{22}); FTIR (KBr): 3310 (N–H), 1632 (C=N), 3300 cm^{-1} (O-H).

(16*E*)-2,6-Dimethyl-N-(7-nitro-2-phenylquinoline-4(1*H*)- ylidene)-5-(phenyl selanyl)pyrimidine-4-amine, 2c: Yield 70%. Anal. Calcd for $C_{27}H_{21}N_5O_2Se$: C, 61.60; H, 4.02; N, 13.30. Found: C, 61.56; H, 4.01; N, 13.26%. FAB mass spectrometry (FAB-MS): *m/z* 528 [M+1]. ^{1}H NMR (400 MHz, $CDCl_3$): δ 2.28 (s, 6H), 6.16 (s, 1H), 6.48 (s, 1H), 6.82 (d, 1H), 6.88 (d, 1H) 6.66-6.72 (m, 5H), 7.25-7.27 (d, 2H), 7.58-7.61 (m, 3H), 9.34 (s, NH); ^{13}C NMR (400 MHz, DMSO-d_6): δ 138.1 (C-2), 102.1 (C-3), 164.4 (C-4), 130.6 (C-5), 110.9 (C-6), 161.4 (C-7), 151.3 (C-8), 148.8 (C-9), 123.2 (C-10), 134.2 (C-11), 126.2 (C-12, C-16), 128.5 (C-13, C-15), 127.8 (C-14). 181. 8 (C-18), 167.8 (C-20), 165.8 (C-22), 110.7 (C-23), 129.8 (C-25), 131.4 (C-26, C-30), 128.6 (C-27, C-28, C-29), 25.3 (CH_3 – C_{20}), 21.2 (CH_3 – C_{22}); FTIR (KBr): 3310 (N–H), 1636 cm^{-1} (C=N).

(16*E*)-2,6-Dimethyl-N-(7-chloro-2-phenyl-quinoline-4(1*H*)-ylidene)-5-(phenyl selanyl)pyrimidine-4-amine, 2d: Yield 72%. Anal. Calcd for $C_{27}H_{21}ON_4Se$: C, 61.60; H, 4.02; N, 13.30. Found: C, 61.56; H, 4.01; N, 13.26%. FAB mass spectrometry (FAB-MS): *m/z* 617 [M+1]; ^{1}H NMR (400 MHz, $CDCl_3$): δ 2.26 (s, 6H), 6.16 (s, 1H), 6.48 (s, 1H), 6.82 (d, 1H), 6.88 (d, 1H) 6.66-6.72 (m, 5H), 7.25-7.27 (d, 2H), 7.58-7.61 (m, 3H), 8.34 (s, NH); ^{13}C NMR (400 MHz, DMSO-d_6): δ 138.1 (C-2), 102.1 (C-3), 164.4 (C-4), 130.6 (C-5), 110.9 (C-6), 161.4 (C-7), 151.3 (C-8), 148.8 (C-9), 123.2 (C-10), 134.2 (C-11), 126.2 (C-12, C-16), 128.5 (C-13, C-15), 127.8 (C-14). 181. 8 (C-18), 167.8 (C-20), 165.8 (C-22), 110.7 (C-23), 129.8 (C-25), 131.4 (C-26, C-30), 128.6 (C-27, C-28, C-29), 25.3 (CH_3 – C_{20}), 21.2 (CH_3 – C_{22}); FTIR (KBr): 3310 (N–H), 1642 (C=N), 740-650 cm^{-1} (C-Cl).

3a: Yield 68%. Anal. Calcd for $C_{31}H_{28}CuN_4O_4Se$: C, 56.15; H, 4.26; N, 8.45. Found: C, 56.12; H, 4.23; N, 8.42%. FTIR (KBr): 1622 (C=N), 540 (Cu–N), 1610 (COO^-), 1380 cm^{-1} (COO^-); FAB mass spectrometry (FAB-MS): 666 *m/z* [M+1]. μ_{eff} (BM) = 1.86; Δ_m (mho cm^2 mol^{-1}) = 18.

3b: Yield 71%. Anal. Calcd for $C_{31}H_{28}CuN_4O_5Se$: C, 54.83; H, 4.16; N, 8.25. Found: C, 54.81; H, 4.14; N, 238. FTIR (KBr): 3305 (O–H), 1622 (C=N), 540 (Cu–N), 1620 (COO^-), 1390 cm^{-1} (COO^-); FAB mass spectrometry (FAB-MS): 682 *m/z* [M+1]. μ_{eff} (BM) = 1.76; Δ_m (mho cm^2 mol^{-1}) = 20.

3c: Yield 66%. Anal. Calcd for $C_{31}H_{27}CuN_5O_6Se$: C, 52.58; H, 3.84; N, 9.89%. Found: C, 52.56; H, 3.81; N, 9.85; FTIR (KBr): 1622 (C=N), 540 (Cu–N), 1610 (COO^-), 1360 cm^{-1} (COO^-); FAB mass spectrometry (FAB-MS): 709 *m/z* [M+1]. μ_{eff} (BM) = 1.96; Δ_m (mho cm^2 mol^{-1}) = 13.

3d: Yield 69%. Anal. Calcd fo r $C_{31}H_{27}CuN_4O_4Se$: C, 53.38; H, 3.90; N, 8.03. Found: C, 53.36; H, 3.86; N, 8.01%. FTIR (KBr): 3305 (O–H), 1622 (C=N), 540 (Cu–N), 1615 (COO^-), 1395 cm^{-1} (COO^-); FAB mass spectrometry (FAB-MS): 698 *m/z* [M+1]. μ_{eff} (BM) = 1.76; Δ_m (mho cm^2 mol^{-1}) = 18.

Results and Discussion

IR spectra

The ligands' IR spectra reveal a ν (C=N) peak between 1654 and 1632 cm^{-1}. Complexes have ν (C=N) bands at 1639-1580 cm^{-1} in their IR spectra[25], which are relocated to lower energy areas compared to free ligands. The change in the energy side of this band is most likely due to an increase in the C=N bond order generated by nitrogen coordination with the copper atoms. Complex spectra show two distinct bands for (COO^-) and (COO^-) at 1630-1600 and 1404-1340 cm^{-1}, respectively. This indicates that the complexes contain the carboxylate oxygen atom. The degree of separation between (COO^-) and (COO^-) is used to define the carboxylate group coordination mode. The separation value between ν_{asy} (COO^-) and (COO^-) in copper complexes was greater than 200 cm^{-1}, indicating that the carboxylate group is coordinated monodentately in the ligands[26]. The appearance of medium intensity bands at 576-578 cm^{-1} and 468-470 cm^{-1}, corresponding to ν (M-O) and ν (M-N), respectively, confirmed complex formation[27]. Table 1 displays the typical peaks of the ligands and complexes. Mass spectra can also provide information about a substance's structure. The mass spectra of the ligand **2c** and its copper complex $[CuL_3(OAc)_2]$ were recorded, and their stoichiometric compositions were compared, as seen in Fig. 1(a) and Fig. 1(b). The intensity of these peaks indicates the ion's stability and abundance[28]. The ligand **2c** shows a molecular ion peak at 556 *m/z*, whereas its copper complex has a

molecular ion peak at 738 *m/z*, showing that the copper complexes are 1:1 stoichiometric. Elemental analysis results are consistent with those estimated from molecular formulas assigned to these complexes, as proven by FAB-mass investigations of individual complexes. Other ligands and copper complexes displayed similar mass spectral characteristics.

^{1}H NMR spectra

The experimental section includes the ^{1}H and ^{13}C NMR spectra of ligands recorded in $CDCl_3$. Ligand **2c** shows (Fig. 1): δ 2.28 (s, 6H), 6.16 (s, 1H), 6.48 (s, 1H), 6.82 (d, 1H), 6.88 (d, 1H), 6.66-6.72 (m, 5H), 7.25-7.27 (d, 2H), 7.58-7.61 (m, 3H) and 9.34 (s, NH). All of the protons were found to be in their predicted locations[29]. The findings of this study add to the support for the bonding mode suggested by their IR spectra. The number of protons calculated from the integration curves and those calculated from predicted CHN analysis values are consistent.

Electronic spectra

The electronic spectra of the ligands and their complexes were recorded in DMSO as a solvent. The ligand's absorption spectra exhibit bands at 224 and 312 nm because of the Schiff base molecule's n–π * and π–π * transitions. The analogous complex's electronic spectra in DMSO show a band at 556 nm that could be attributed to the 2B1g → 2A1g transition[30,31]. This band can be attributed to the 2B1g → 2A1g transition and is suggestive of the square planar environment surrounding the copper (II) ion. The same spectral properties were assigned to other compounds. In the electronic spectra of all the complexes, the secondary band of the benzene, the π – π * transition of the benzenoid / or n– π * (COO), the π – π * transition of the > C=N- chromophore, and the n–π * transition of the > C=N- chromophore exhibit bands in the 200–225, 272–332 and 362–390 nm ranges. Additionally, the complexes' spectra showed a few distinct lines in the 233–257 nm range that might represent bands for charge transfer. Magnetic susceptibility tests showed that the copper complexes were paramagnetic at RT. These complexes' magnetic moments are strikingly similar to those of copper (II) complexes in which there is no metal–metal interaction. The complex **3c**'s magnetic moment at RT is 1.86 BM, which is typical of mononuclear complexes of magnetically diluted d^9 systems with a square planar structure and S = 1/2 spin state that do not exhibit metal–metal interaction along the axial position. The magnetic characteristics of other copper complexes were similar (Fig. 2).

Table 1 — IR characteristic peaks of synthesized ligands and complexes

Ligand / Complex	ν C=N (cm^{-1})	ν M-N (cm^{-1})	ν $(COO^-)_{ass}$ (cm^{-1})	ν $(COO^-)_{sy}$ (cm^{-1})
2a	1635	–	–	–
2b	1630	–	–	–
2c	1622	–	–	–
2d	1629	–	–	–
3a	1625	520 – 550	1615	1380
3b	1620	530 – 550	1610	1370
3c	1610	520 – 550	1600	1390
3d	1620	530 – 550	1610	1370

ESR spectra

ESR spectra of copper chelate (Fig. 3) obtained in DMSO solution at 77 K. The metal-ligand link was determined to be a covalent[32] with a g|| value of 2.262. Due to regular geometrical configurations (f = g||/A||), the planar distortion of copper (II) chelate was calculated to be 146.2. The findings showed that the distortion brought about by regular square planar geometry around the copper center[33] aided the biomolecular mechanism for biological processes.

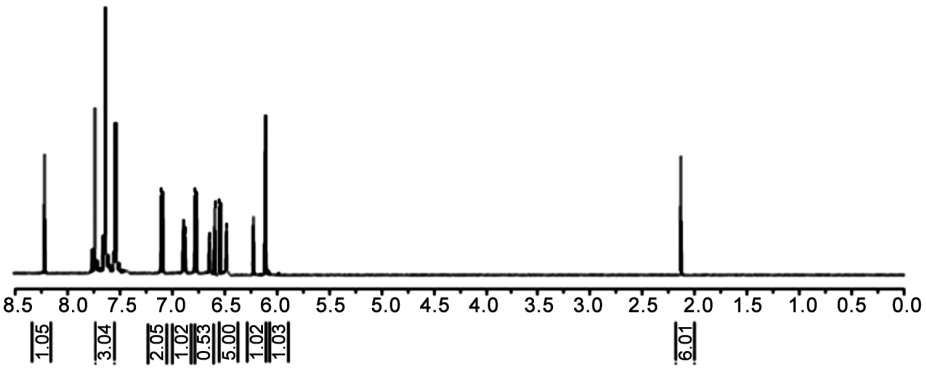

Fig. 1 — ^{1}H NMR spectrum of L_{2c}

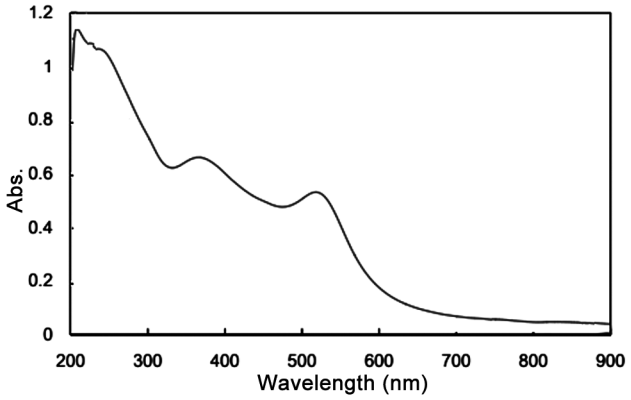

Fig. 2 — UV spectrum of **3a**

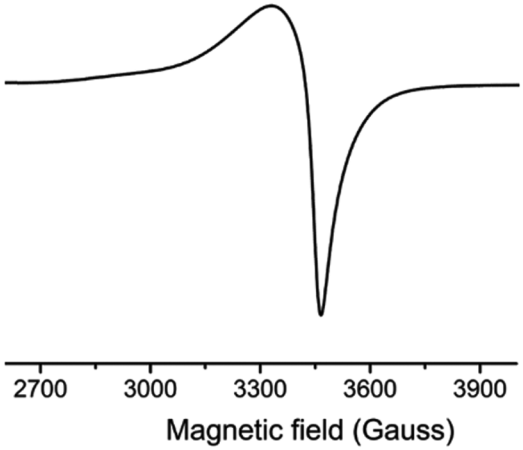

Fig. 3 — ESR spectrum of **3d**

Molar conductance

The molar conductance data for the copper complexes measured in DMSO solution were found for the 0.001 M solutions in the experimental section. Within the anticipated range of 1 to 35 mho cm^2 mol^{-1} for non-electrolytes[34], the complexes' values ranged from 10 to 29 mho cm^2 mol^{-1}. The complexes are non-electrolytic due to the acetate groups' coordination participation. This was verified by a chemical study of the $CH3COO^-$ ion that was not precipitated by the addition of $FeCl_3$.

TGA and DTA studies

The complex is stable up to 250°C, with no weight loss occurring before this temperature, according to the Cu (II) complex's TGA and DTA curves (Fig. 4). The loss of one chlorine atom at 250°C marked the start of the first stage of deterioration, which led to an 11.95% decrease in functional weight. Further breakdown of the resulting complex at 291°C led to the loss of the phenyl moiety, which resulted in a

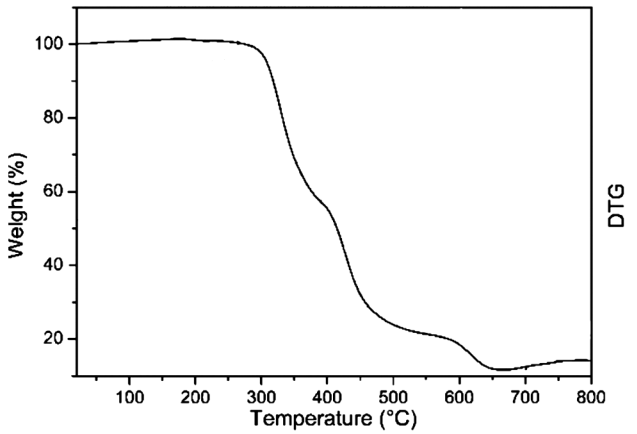

Fig. 4 — Thermogravimetric Profile of **3d**

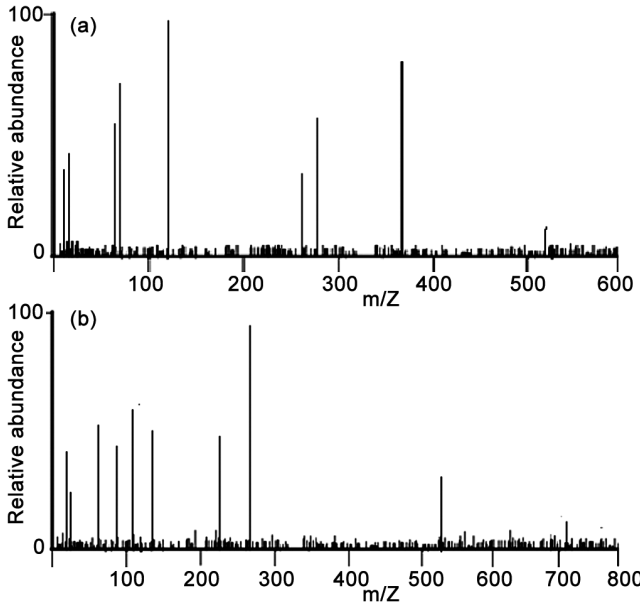

Fig. 5 — (a) Mass spectrum of ligand **2c** and (b) Mass spectrum of copper complex **3c**

11.40% functional weight loss. The third step of breakdown at 340°C resulted in the loss of the quinoline moiety, which led to a 47.95% reduction in weight. Additionally, the molecule lost its remaining organic moiety, causing it to dissolve up to 492°C. The residue's final weight is cupric oxide.

Mass spectra

Mass spectra can also be used to determine a substance's structure. Fig. 5(a) and Fig. 5(b) display the stoichiometric compositions of the ligand **2c** and its copper complex $[CuL_3(OAc)_2]$ after their mass spectra were recorded. The intensity of these peaks reflects the abundance and stability of the ion. The

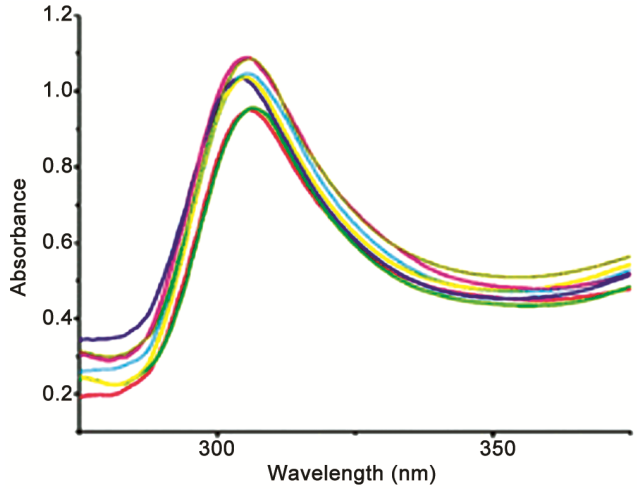

Fig. 6 — UV–Vis absorption spectra of copper complex **3c** by the addition of DNA (CT-DNA, in DMF, tris–HCl buffer, *p*H 7.3) upon addition of CT-DNA=0.5 µm, drug =10 µm, 20 µm; 30 µm; 40 µm; 50 µm

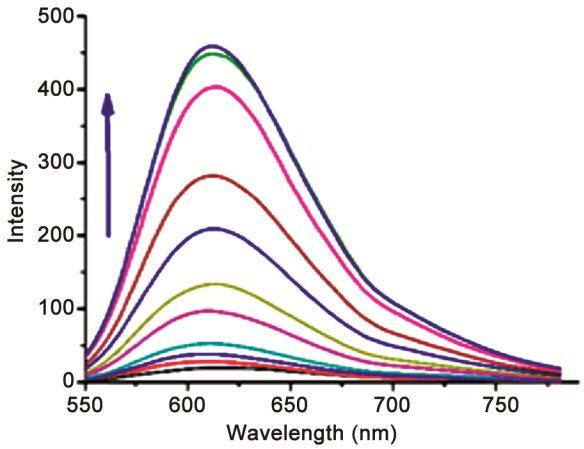

Fig. 7 — Fluorescence emission of copper complex **3c** in Tri-HCl buffer. Fluorescence intensity increasing CT-DNA concentrations (5 µL, 10 µL, 15 µL, 20 µL). Inset: plots of relative emission intensity *versus* [DNA]/[complex]

copper complexes exhibit 1:1 stoichiometry, as evidenced by the ligand **2c** having a molecular ion peak at 528 *m/z* and its copper complex having a molecular ion peak at 709 *m/z*. FAB-mass analyses of individual complexes show that the elemental analysis values are similar to those estimated from molecular formulas attributed to these complexes. Other ligands and their copper complexes were assigned similar mass spectrum characteristics.

DNA binding studies

Absorption spectral studies

One of the best experimental methods for examining the interactions between metal ions and DNA in metal complexes was electronic absorption spectroscopy. Because aromatic chromophores and CT-DNA base pairs have a strong stacking relationship, intercalation with DNA typically causes hypochromism and bathochromism[35]. The absorbance of compound **3c** is clearly resolved at 289 nm, as seen by the absorption spectra. Because more stable compounds were formed, increasing the concentration of CT-DNA produced hypochromic and bathochromic increases in its visible absorption spectra. Complex **3c** showed a drop in intensity as CT-DNA concentrations increased. Its highest red-shift absorption peak (Fig. 6) showed a shift towards higher wavelengths hypochromicity (about 11%) and bathochromic changes (maximum: 21.1 nm). Complex **3c** binds strongly to CT-DNA through intercalation36, as demonstrated by the intrinsic binding constants (Kb), which were determined to be 3.9×10^5 M^{-1} using the change in absorbance values with increasing amounts of CT-DNA[36].

Fluorescence studies

Complex **3c** generates luminescence in Tris buffer, peaking at 450 nm at RT (*p*H 7.0–7.2). When calf thymus DNA (CT DNA) is introduced to the complex, the emission intensity rises in comparison to the complex's intensity alone (Fig. 7). It has been shown in the past that the presence of additional molecules may at least slightly reduce this enhanced fluorescence. Because the hydrophobic environment within the DNA helix limits the accessibility of solvent water molecules to the duplex and consequently, limits complex mobility at the binding site, this suggests that the copper complex interacts strongly with CT-DNA *via* intercalation and will be effectively shielded by DNA. This results in a reduction of vibrational modes of relaxation[37], which raises the degree of enhancement of the copper complex and is consistent with the absorption spectra. Measurements of viscosity and absorption spectra confirmed the order of increase in complex emission rate.

Viscosity measurements

The copper complex's binding mechanisms with CT-DNA were clarified by the viscosity data. The most important tests of binding in solution, when crystallographic structural data is not available, are hydrodynamic assays that are sensitive to changes in length (*e.g.*, sedimentation, viscosity)[38]. Due to an increase in base pair separation at intercalation

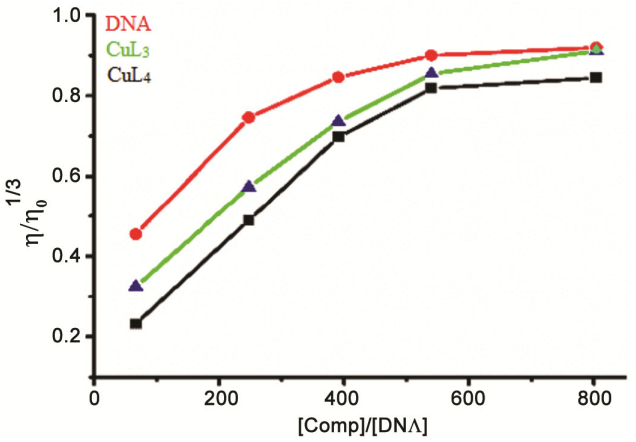

Fig. 8 — Effect of the Cu(II) complexes ([CuL_3] and [$Cu(L_4)$] on the relative viscosities of CT-DNA

sites and, consequently, an increase in total DNA length, a standard intercalative mode significantly increases the viscosity of DNA solution. A chemical that binds largely in the DNA grooves *via* partial and non-classical intercalation, on the other hand, typically causes a negative or no shift in DNA solution viscosity under identical conditions. Viscosity measurements on CT-DNA were performed by varying the complex concentration to better understand the current complex's binding mode. Fig. 8 shows how the complex affects the viscosity of rod-like DNA. The viscosity of DNA rises as the concentration of complex **3c** increases. According to the findings, the complex's presence has a noticeable effect on CT-DNA relative viscosity.

Cholinesterase inhibitory activity

Cholinesterase inhibitors (ChEIs) are a type of medication that increases cholinergic activity in the brain, which improves memory, efficiency, and reduces psychiatric and behavioral disorders. The AChE and BuChE inhibitory activities of the synthesized phenylselanylquinoline derivatives were measured using a modified Ellman technique[39] and compared to Galantamine and Rivastigmine as standards. Some acetylcholinesterase inhibitors (donepezil, galantamine, and rivastigmine) were used to treat Alzheimer's disease symptoms. Table 2 shows the IC_{50} values for AChE and BuChE inhibitors. The strongly conjugated phenylselanylquinoline derivative **2c**, like regular Galantamine (IC_{50} = 2.40 μM), displayed the strongest inhibition against AChE (IC_{50} = 0.20 μM) and Rivastigmine (IC50 = 3.01 μM). The IC_{50} values revealed that phenylselanylquinoline compounds, unlike Galantamine, selectively inhibit AChE *via* a

Table 2 — Computational output of receptor- ligand docking

Ligand	Ligand with acetylcholinesterase		
	Binding Affinity (kcal/mol)	rmsd/lb	rmsd/ub
2c	–11.6	0	0
2c	–11.1	4.852	2.01
2c	–11	6.598	2.186
2c	–10.9	5.527	2.458
2c	–10.8	7.226	2.763
2c	–10.7	2.26	1.419
2c	–10.6	4.846	1.129
2c	–10.4	4.968	3.061
2c	–10.4	2.366	1.811
2c	–10.6	0	0
2c	–10.1	4.112	2.522
2c	–10.1	6.945	3.021
2c	–10	5.765	3.166
2c	–9.7	3.653	1.892
2c	–9.4	6.559	2.433
2c	–9.3	4.37	2.785
2c	–9.3	7.352	3.328
2c	–8.8	6.214	2.794

hydrophobic interaction and π-π interactions. The aromatic center illuminates fused aromatic nuclei with higher inhibitory AChE potencies compared to similar molecules with only one or two fused ring systems. The most effective AChE inhibitors are those with fused aromatic characteristics. The azomethine moiety also increases strong binding to the AChE active site, thereby suppressing cholinesterase substrate hydrolysis. As a result, azomethine, quinoline, and lipophilic moieties on conjugated aromatic centers may be the major requirements for anti-AChE activity.

Molecular Docking

AutoDock Vina generates two output files at the end of its run, an auto dock structure file with ten different docking poses of the considered ligand, and another with binding affinity and two variants of Root Mean Square Deviation (RMSD) metrics such as rmsd/lb (RMSD lower bound) and rmsd/ub (RMSD upper bound) of all nine ligand confirmations, as shown in Table 2.

AutoDock Vina, by default sorts the dock score or binding affinity of the nine different docking poses of ligand from the lowest best to highest worst. From the obtained outcomes, it was observed that when the ligand docked with acetyl cholinesterase, attained best least docking affinity was -11.6 (kcal/mol) with zero rmsd/lb and rmsd/ub.

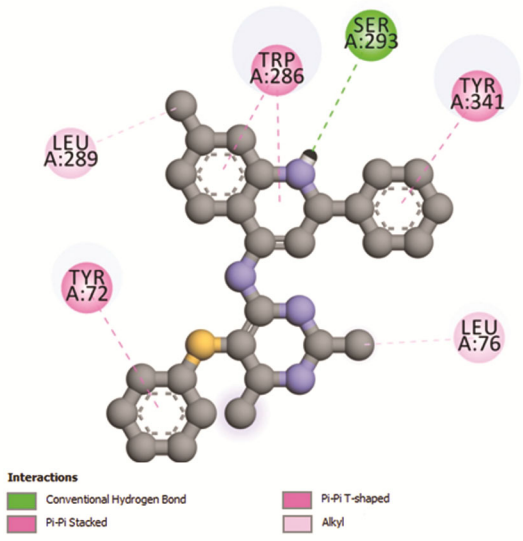

Fig. 9 — Depiction of acetylcholinesterase-ligand L_{2c} complex

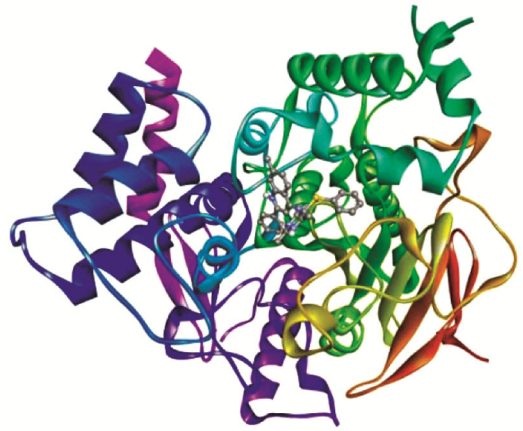

Fig. 10 — Hydrophobic interaction of acetylcholinesterase-Ligand **2c** (2D depiction)

The acquired receptor ligand complexes were analyzed using the BIOVIA Discovery Studio visualizer. There is a provision for loading the ligand posture with the best dock score. First, acetylcholinesterase and its best ligand confirmation were placed into the workspace, and the receptor and ligand were identified. Then the receptor-ligand interaction was enabled and examined. Fig. 9 displays the expected binding site of acetylcholinesterase with the ligand molecule.

Fig. 10 depicts the hydrophobic interaction of acetylcholinesterase in both two and three dimensions. Acetylcholinesterase interacts with ligand molecules primarily through its aromatic amino acid residues. Fig. 10 demonstrated interactions. TrpA:286, SerA:298, TyrA:341, LeuA:289, TyrA:72, LeuA:76, and ligand. SerA:286 exhibited hydrogen bond contact, TrpA:341, TrpA:286, TyrA:72 demonstrated π-π interaction, and LeuA:289 and LeuA:76 demonstrated π-alkyl interaction. Fig. 9 displays the receptor/ acetylcholinesterase interfaces in terms of several characteristics at the binding site. It depicts the aromatic surface, with aromatic ring edges designated in blue and faces in orange, indicating that the majority of the residues involved in interactions are aromatic. It also depicts the H-bond surface, with acetylcholinesterase active site donors in magenta and acceptors in green, hydrophilic regions in blue, and acidic areas in red. Highly exposed areas for solvent interaction are shown in blue, while hydrophobic internal buried regions are represented in green.

Conclusion

This study examined the synthesis, characterization, and biological evaluation of copper (II) complexes with organoselenium-based Schiff base ligands (16E)-2,6-dimethyl-N-(2-phenylquinoline-4(1H)-ylidene)-5-(phenylselanyl) pyrimidine-4-amine. Spectroscopic analysis reveals that the complex is linked to two carboxylate oxygen atoms and a copper atom by the quinoline moiety and organoselenium from the ligand. The analytical and spectral results show that all copper complexes have a deformed square planar shape with a metal-to-ligand ratio of 1:1. Absorbance, fluorescence, and viscosity tests were performed to assess the copper complexes' binding to calf thymus DNA (CT-DNA). All of the complexes interacted with CT-DNA in an intercalation manner. According to the findings. *In silico* molecular docking of ligands with acetylcholinesterase was carried out separately using AutoDock Vina. When docked with acetylcholinesterase, ligand **2c** has a desirable minimum optimum interaction energy of -10.6 kcal/mol. Docking studies revealed that the majority of aromatic amino acid residues, including Phe, Tyr, and Trp, are located near the active site of acetylcholinesterase and interact with the ligand. Further research is needed to determine whether the ligand can be used to inhibit the function of acetylcholinesterase and thus prevent the occurrence of Alzheimer's disease.

Acknowledgement

The authors thank the Mepco Schlenk Engineering College, Sivakasi for providing the necessary facilities. This research did not receive any specific grant from funding agencies in the public, commercial, or not-for-profit sectors

References

1 De Oliveira C, Brum J, Neto D C F, De Almeida J S F, Lima J A, Kuca K, França T C C & Figueroa-Villar J D, *Int J Mol Sci*, 20 (2019) 3944.

2 Fiorito J, Saeed F, Zhang H, Staniszewski A, Feng Y, Francis Y I & Arancio O, *Euro J Med Chem*, 60 (2013) 285.

3 Abdel-Rahman L H, Abu-Dief A M, Aboelez M O & Abdel-Mawgoud A A H, J *Photochem Photobiol*, 170 (2017) 271.

4 Abdel-Rahman L H, Abu-Dief A M & Abdel-Mawgoud A A H, *Int J Nano Chem*, 5 (2019) 1.

5 Abdel-Rahman L H, Abu-Dief A M, Shehata M R, Atlam F M & Abdel-Mawgoud A A H, *App Organomet Chem*, 33 (2019) 4699.

6 Abdel-Rahman L H, Abu-Dief A M, Moustafa H & Abdel-Mawgoud A A H, *Arab J Chem*, 13 (2020) 649.

7 Abdel-Rahman L H, Abu-Dief A M, Adam M S S & Hamdan S K, *Catal Lett*, 146 (2016) 1373.

8 Al-Saeedi S I, Abdel-Rahman L H, Abu-Dief A M, Abdel-Fatah S M, Alotaibi T M, Alsalme A M & Nafady A, *Catalysts*, 8 (2018) 452.

9 Adam M S S, Abdel-Rahman L H, Abu-Dief A M & Hashem N A, *Inorg Nano-Met Chem*, 50 (2020) 136.

10 Huijbregts S C J, De Sonneville L M J, Van Spronsen F J, Berends I E, Licht R, Verkerk P H & Sergeant J A, *Neuropsychology*, 17 (2003) 369.

11 Lee E S, Choi B W, Jung D I, Hwang H J, Han J T & Lee B H, *B Korean Chem Soc*, 24 (2003) 243.

12 Fisher A, *J Neurochem*, 120 (2012) 22.

13 Chan K Y, Wang W, Wu J J, Liu L, Theodoratou E & Car J, *The Lancet*, 381 (2013) 2016.

14 Anand P, Singh B & Singh N, *Bioorg Med Chem*, 20 (2012) 1175.

15 Somani G, Kulkarni C, Shinde P, Shelke R, Laddha K & Sathaye S, *J Pharm Bioallied Sci*, 7 (2015) 32.

16 Tardito S & Marchio L, *Curr Med Chem*, 16 (2009) 1325.

17 Wessjohann L A, Schneider A, Abbas M & Brandt W, *Bio Chem,* 388 (2007) 997.

18 May S W & Pollock S H, *Drugs*, 56 (1998) 959.

19 Mugesh G, du Mont W W & Sies H, *Chem Rev*, 101 (2001) 2125.

20 Marzano C, Pellei M, Tisato F & Santini C, *Anti Cancer Agents Med Chem*, 9 (2009) 185.

21 Santini C, Pellei M, Gandin V, Porchia M, Tisato F & Marzano C, *Che Rev*, 114 (2014) 815.

22 Zeglis B M, Pierre V C & Barton J K, *Chem Comm*, 44 (2007) 4567.

23 Gil A, Melle-Franco M, Branchadell, V & Calhorda M J, *J Chem Theory Comp*, 11 (2015) 2714.

24 Adhikary C, Bera R, Dutta B, Jana S, Bocelli G, Cantoni A & Koner S, *Polyhedron*, 27 (2008) 1556.

25 Nakamoto. K, *Spectroscopy and Structure of Metal Chelate Compounds* (John Wiley, New York) (1988).

26 Geary W J, *Coord Chem Rev*, 7 (1971) 81.

27 M Hamming M & Foster N, *Interpretation of Mass Spectra of Organic Compounds*, (Academic Press, New York, John Wiley & Sons Ltd) 1972.

28 Liu Y J, Wang N, Mei W J, Chen F, He L X, Jian L Q & Wu F H, *Transit Met Chem*, 32 (2007) 332.

29 Chandra S & Gupta L K, *Spectrochim Acta A Mol Biomo Spectro*, 61 (2005) 269.

30 Lever A B P, *Inorganic Electronic Spectroscopy*, 2nd Ed. (Elsevier, New York) 1968.

31 Gaballa A S, Asker M S, Barakat A S & Teleb S M, *Spectrochim Acta A Mol Biomo Spect*, 67 (2007) 114.

32 Fujiwara M. Wakita H, Matsushita T & Shono T, *Bull Chem Soc Jpn*, 63 (1990) 3443.

33 Geary W J, *Coord Chem Rev*, 7 (1971) 81.

34 Anjaneyulu Y & Rao R P, *Synth React Inorg Met Org Chem*, 16 (1986) 257.

35 Prabhakara M C, Naik H B, Krishna V & Kumaraswamy H M, *Nucleo Nucleo Nuc Aci*, 26 (2007) 459.

36 Lamani D S, Reddy K V, Naik H B, Naik H P & Naik L R, *Phosp Sul Sil*, 185 (2010) 550.

37 Prakash Naik H R, Bhojya Naik H S, Ravikumar Naik T R, Naik H R, Lamani D S & Aravinda T, *J Sulp Chem*, 29 (2008) 583.

38 Vaidyanathan V G & Nair B U, *J Inorg Biochem*, 95 (2003) 334.

39 Pohanka M, *Biomed Pap Med Fac Palacky Uni Olo*, 155 (2011) 219.